L.O. Copy Mr. R.J. Templin.

L.O. NAE 225-5 FILE BM49-10R-1 PREPARED BY JGL & DWB CHECKED BY JL	NATIONAL AERONAUTICAL ESTABLISHMENT OTTAWA CANADA LABORATORY MEMORANDUM SECTION Aerodynamics	AE-46e NO. HSAL-M-59 PAGE 1 OF 16 COPY NO. 4 DATE 24 Oct. 1955

SECURITY CLASSIFICATION ~~SECRET~~

SUBJECT Supersonic tunnel tests on effects of engine-off operation on lateral characteristics of the C-105 aircraft.

PREPARED BY J. G. LaBerge
D. W. Boyer

ISSUED TO Mr. J. H. Parkin
Dr. D. C. MacPhail
Mr. J. R. Templin (2)
Mr. J. Lukasiewicz (2)
Authors (2)
Aero Library (2)
Mr. J. Chamberlain, Avro Aircraft (3)

Summary

The effect of blocking completely or partially one engine intake on the side force and yawing moment of the C-105 aircraft was investigated at supersonic speeds. A 1/80 scale model was tested in the 10 inch tunnel, the force and moment measurements being taken at a Mach number of 2.04. Schlieren photographs are presented for Mach numbers of 1.64 and 2.04.

Over the whole range of yaw angles explored complete blockage of one intake resulted in a yawing moment ($\Delta C_n = 0.001$) tending to put the blocked intake on the windward side of the fuselage.

Contents

	Page
List of Illustrations	4
List of Symbols	5
1. Introduction	7
2. Test Model	7
3. Wind Tunnel	7
4. Balance and Model Mounting	8
5. Test Procedure	9
6. Reduction of Data	10
6.1 Side Force and Yawing Moment	10
6.2 Mass Flow Ratio	11
7. Discussion of Results	12
7.1 Mass Flow Ratio	12
7.2 Pressure Recovery	13
7.3 Base Pressure	13
7.4 Yawing Moment	13
7.5 Side Force	14
7.6 Schlieren Photographs	14
7.7 cp Travel	15
8. Conclusions	15
Table I	

List of Illustrations

	Figure
Diagram of 1/80 Scale Model	1
Wave Interference on Model at $M_\infty = 2.04$	2
Typical Recorder Traces of Moment Measurements	3
Mass Flow Ratio vs. Angle of Yaw	4
Pressure Recovery vs. Angle of Yaw	5
Base Pressure vs. Angle of Yaw	6
C_n vs. Angle of Yaw	7
C_Y vs. Angle of Yaw	8
Schlieren Photographs, $M_\infty = 1.64$, $\psi = 0°$	9
Schlieren Photographs, $M_\infty = 1.64$, $\psi = -2°$	10
Schlieren Photographs, $M_\infty = 1.64$, $\psi = -4°$	11
Schlieren Photographs, $M_\infty = 1.64$, $\psi = -5°$	12
Schlieren Photographs, $M_\infty = 2.04$, $\psi = 0°$	13
Schlieren Photographs, $M_\infty = 2.04$	14
Schlieren Photographs, $M_\infty = 2.04$, $\psi = +2°$	15
C_Y vs. C_n	16
cp Travel Due to Intake Blockage	17

List of Symbols

A	Cross-sectional area, $in.^2$
a	Distance between cp and balance RC with long sting, in.
b	Span of model, 7.50 in.
CG	Center of gravity of model located $0.28\bar{C}$ downstream of leading edge of mean aerodynamic chord
C_n	$\frac{n_{CG}}{qSb}$, yawing moment coefficient
C_Y	$\frac{Y}{qS}$, side force coefficient
$\bar{C}$	Wing mean aerodynamic chord, 4.53 in.
cp	Side force center of pressure
d	Distance between RC and CG with short sting, 1.55 in.
γ	Ratio of specific heats, $C_p/C_v = 1.4$
h	Distance between RC and CG with long sting, 0.31 in.
ℓ	Distance between cp and RC with short sting, in.
m	Mass flow, slugs/sec.
mV	Millivolts
M	Mach number
n	Yawing moment, lb. in.
p	Static pressure, psia.
p_o	Total pressure, psia
q	Dynamic pressure, $\frac{\gamma}{2} pM^2$, psia
ρ	Density
RC	Resolving center of balance
S	Wing gross area, $27.6\ in.^2$
V	Velocity ft./sec.

List of Symbols (Concluded)

x Longitudinal distance, in.

Y Side force, lbs.

Subscripts

∞ Free stream conditions

b Base of rubber plug

CG With respect to the model center of gravity

e Intake duct exit

i Intake duct entry

L With long sting

s With short sting

sh Sting shield

Superscripts

$( )^{*}$ Critical conditions

1. Introduction

A 1/80 scale model of the C-105 aircraft was tested in the 10 inch tunnel in order to determine the effect of mass flow changes in one intake on the lateral stability at supersonic speeds. Only the zero lift case was considered. The model was made for testing in the 30 inch tunnel and was therefore too large for the 10 inch tunnel. However, by removing the vertical tail and by taking the moment measurements at a Mach number of 2.04 the wave interference was reduced to a minimum.

Inasmuch as that region of the model in the vicinity of the intakes was interference-free, schlieren photographs were taken at M_∞ = 2.04 and 1.64.

The test Reynolds number was about 1.5×10^6 based on the mean aerodynamic chord.

2. Test Model

The model tested, supplied by Avro Aircraft Ltd., did not incorporate the latest design revisions, e.g. the wing being that with the basic leading edge 8% notches. A sketch of the model showing pertinent dimensions is given in Figure 1.

In order to vary the mass flow through an intake, rubber plugs were inserted in the duct exit. A solid plug produced the no flow condition whereas a drilled plug gave a mass flow corresponding to an exit area equal to approximately half the fully open area.

The vertical fin having been removed, the recessed area of the fuselage thereby exposed was filled with plasticine and smoothed over.

3. Wind Tunnel

Because of the urgency of the test program and the unavailability of a suitable balance, the model could not be tested in the 30 inch tunnel. Rather, it was mounted in the 10 inch tunnel and tested at nominal Mach numbers of 1.6 and 2.0. Even after removal of the vertical fin it was found by schlieren observation that the model was subject to severe interference from shock wave reflection at the lower Mach number. However, at the higher Mach number interference was limited to the intersection of the expansion waves from the nozzle exit with the model wing tips, see Figure 2. It was felt that these effects would be sufficiently small so as not to invalidate the comparative nature of the results.

The nominal and mean Mach numbers as well as the percent variation of the Mach number in the tunnel working section are given in the table below.

M - Nominal	1.6	2.0
M - Mean	1.64	2.04
% M	±0.9	±1.5

The tunnel intake air was at approximately atmospheric conditions and was dried to a specific humidity of about 0.0005. In the case of force and moment measurements tunnel runs of about 7 seconds duration were taken.

4. Balance and Model Mounting

The model was mounted at zero lift on a side force and yawing moment balance. This balance was of the sting type with a displacement transducer pick-up in the balance housing below the tunnel jet. From the moments measured about the balance pivot point with two stings of different lengths, the side force could be deduced. Knowing the distance between the balance pivot point i.e. the resolving center, and the model center of gravity, the yawing moment about the latter point could then be simply calculated.

The stings were protected from the air stream by means of shields.

A short hardened steel adaptor was fitted between the model exhaust ducts and wedged into the after part of the fuselage. The other end of the adaptor was simply screwed into the balance stings. Two small plastic wedges were bonded to the sides of the adaptor in such a manner as to deflect the flow from the intakes outward and away from the sting face. This was necessary to prevent interference of intake air flow on the moment measurements.

The balance could provide angles of yaw from +2° to -5° in steps of 1°.

Inasmuch as the parallel beam of the schlieren system was horizontal it was necessary to rotate the model through 90° in order to take photographs of the flow configurations at the intake entries. For this purpose a drag balance was used to support the model at zero incidence and at the same time provide a range of yaw angles by means of the incidence gear. Thus yaw angles between -3° and +3° were provided which could be increased to -9° with the use of shims under the balance housing.

5. Test Procedure

Engine failure was simulated by plugging the duct exit, a solid rubber plug as well as a half open one (see section 2 above) being used. At a given angle of yaw, measurements were taken for the fully open, half open and fully closed duct exits, the starboard and port ducts being considered successively. The following system was adopted to identify the various duct exit configurations.

Constant Angle of Yaw

Designation	Port Duct	Starboard Duct
0/0	Fully open	Fully open
0/½	Fully open	Half open
0/C	Fully open	Fully closed
C/0	Fully closed	Fully open
½/0	Half open	Fully open

Thus the interchange of plugs between port and starboard ducts at constant angle of yaw produced the same effect as a change in sign of the angle of yaw with the plug left in one duct.

The following tests were carried out at a Mach number of 2.04 and for an angle of yaw range of +2° to -5° in steps of 1°.

(a) Moment measurements with short and long stings for all the duct exit configurations shown in the above table. Transducer outputs were led to a high-speed potentiometer recorder with which reading accuracies up to ±0.2% could be achieved. Typical recorder traces are shown in Figure 3. Shield pressures were read on a mercury manometer.

(b) Mass flow and total pressure recovery in a fully open duct with the other duct successively fully open, half open and fully closed; mass flow and total pressure recovery in a half open duct with the other duct fully open. In both cases, measurements were made in the port as well as in the starboard duct. These measurements were obtained by means of a 1/16 in. O.D. pitot probe inserted about a quarter of an inch into the duct exit and on the duct axis. The probe was fastened to the sting shield and was connected to a pressure transducer outside the tunnel. The output of this transducer was led to a second recorder.

(c) Base pressure measurements. These were made with the pitot probe positioned about 1/32 inch behind the rubber stopper of a fully closed duct, the other duct being fully open. The probe arrangement is shown schematically in the inset in Figure 6. Base pressures were thus measured on both the port and starboard sides and for both long and short stings.

Sample schlieren photographs taken at Mach numbers of 1.64 and 2.04 for some of the above exit duct configurations are shown in Figures 9 to 15 inclusive. Time did not permit the investigation of angles of yaw beyond 3° at a Mach number of 2.04. In interpreting these photographs it should be noted that the starboard duct is at the bottom and that positive yaw is counterclockwise.

6. Reduction of Data

6.1 Side Force and Yawing Moment

From the moments, with respect to the balance resolving center (RC), measured with the short and long stings, the side force and the yawing moment about the model CG were determined as follows:

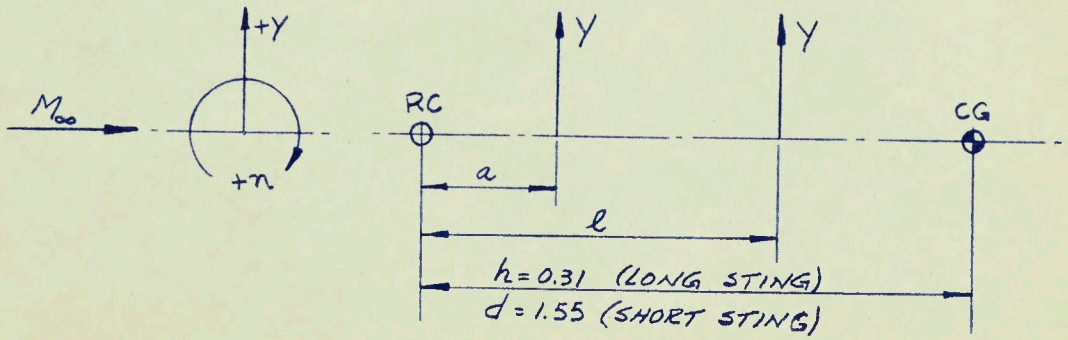

where

$\ell - a = d - h = 1.24$ in. = difference in sting lengths
h = the distance between RC and CG with long sting
d = the distance between RC and CG with short sting

also let

n_L = yawing moment about RC with long sting
n_s = yawing moment about RC with short sting

since

$n_L = -aY$ and $n_s = -\ell Y$

it follows that

$$Y = \frac{n_L - n_s}{1.24} \qquad (1)$$

also

$$n_{CG} = (h-a)Y = (h + \frac{n_L}{Y})Y$$

Hence

$$n_{CG} = 0.31\,Y + n_L \qquad (2)$$

The equivalent expression in terms of n_s is

$$n_{CG} = 1.55\,Y + n_s \qquad (2a)$$

6.2 Mass Flow Ratio

If it is assumed that the intake exit is choked, the mass flow through the intake becomes

$$m_e = A_e \rho_e V_e = A_e \rho^* V^* \qquad (3)$$

Define

$$m_\infty = A_i \rho_\infty V_\infty \qquad (4)$$

i.e. The mass flowing in the free-stream through an area equal to that of the intake entry area.

The mass flow ratio then becomes,

$$\frac{m_e}{m_\infty} = \frac{A_e}{A_i} \frac{\rho^* V^*}{\rho_\infty V_\infty} \qquad (5)$$

which can be shown to be equivalent to

$$\frac{m_e}{m_\infty} = \frac{A_e}{A_i}\,\frac{p_{oe}}{p_{o\infty}}\,\frac{1}{M_\infty}\left(\frac{2}{\gamma+1} + \frac{\gamma-1}{\gamma+1}\,M_\infty^2\right)^{\frac{\gamma+1}{2(\gamma-1)}} \qquad (6)$$

For $M_\infty = 2.04$, eq.(6) reduces to

$$\frac{m_e}{m_\infty} = 1.745\,\frac{A_e}{A_i}\,\frac{p_{oe}}{p_{o\infty}} \qquad (7)$$

The area ratios corresponding to the fully open and the half open duct exit configurations are given in the table below.

Configuration	A_e/A_i
Fully open	1.074
Half open	0.402

All test and reduced data for $M_\infty = 2.04$ are reproduced in Table 1.

7. Discussion of Results

7.1 Mass Flow Ratio

Mass flow ratio, as determined by Eq. 7, is plotted against angle of yaw in Figure 4. As was to be expected the mass flow through the windward intake increased while that through the leeward duct decreased with increasing angle of yaw. Evident in the figure was an apparent lack of symmetry of the two intakes, for with reciprocal duct exit configurations (e.g. C/O and O/C) the mass flow ratios were equal at an angle other than zero yaw.

Also evident was the large reduction in the mass flow through one intake when the other intake was changed from fully open to fully closed. It is apparent therefore, that, in the absence of leaks between the ducts, the mass flows through the ducts were not independent.

The mass flow through the port duct decreased progressively as the starboard duct was progressively closed; however, in the

case of the starboard duct, the mass flow through it first increased and then decreased when the port duct was progressively closed. This again would point to mass flow interdependence.

7.2 Pressure Recovery

It will be seen in Figure 5, which shows total pressure recovery versus angle of yaw, that the pressure recovery was quite low, never exceeding 0.6 over the range of yaw angles tested. This was attributed mainly to the friction losses in the relatively long intake ducts.

The points advanced in the previous section apply equally well here in view of the relationship between pressure recovery and mass flow ratio (Eq.7).

7.3 Base Pressure

As described earlier, the base pressure was understood to refer to the pressure at the base of a solid rubber plug introduced into the duct exit. Knowing this pressure, corrections to the yawing moment could be made to account for other known jet pressures.

The base pressure referred to free-stream stagnation pressure is shown plotted against angle of yaw in Figure 6. Here again some flow asymmetry was present for the base pressure on the starboard side was greater than on the port side, being about 10% larger at zero yaw. Furthermore, the base pressure was dependent on model location in the working section there being an increase again of about 10% in base pressure when the model was transferred from the long to the short sting. This was attributed to the effect of the expansion waves issuing from the nozzle exit as shown in Figure 2.

7.4 Yawing Moment

This is given in Figure 7 for yaw angles between +2° and -5°. It will be seen that, for all duct exit configurations and angles of yaw, the simulated shutting down of one engine produced a yawing moment tending to rotate the engine to windward. However, the fact that the half open duct configuration produced a larger effect on yawing moment than the fully open duct configuration could not be simply explained. The completely closed intake case contributed a change in C_n of about 0.001.

It would appear from Figure 7 that the model was slightly misaligned (by 0.5°) in the yaw plane with respect to the

airstream direction. This misalignment was not responsible, however, for the observed asymmetry in the mass flow ratio and pressure recovery curves in Figures 4 and 5. Rather, taking into account the model misalignment given by Figure 7 would tend to increase the apparent asymmetry shown in Figures 4 and 5.

7.5 Side Force

The side force coefficient exhibited a large amount of scatter when plotted against angle of yaw, Figure 8, whereas the yawing moment coefficient was relatively free of scatter, Figure 7. Part of the reason for this increased scatter is due to the fact that the side force, Eq.1, is from 3 to 4 times more sensitive to measuring errors than the yawing moment, Eq.2a. Because of the unsteadiness of the recorder traces, Figure 3, n_L and n_s could not be measured to better than about ± 0.05 lb.in. Moreover, presumably because of model vibration, repeatability of the results was very poor at small angles of yaw, as can be seen in Table 1.

Nevertheless some conclusions can be drawn from Figure 8. It will be seen that at all angles of yaw a completely closed intake produced a side force increment, positive for closed starboard intake and negative for closed port intake. The increment in C_Y was more variable over the yaw angle range than that in C_n but averaged between 0.002 and 0.003.

At negative angles of yaw the effect on side force of partial mass flow through the intakes was intermediate between the effects of full mass flow and no mass flow, as was to be expected. At positive yaw, however, the partial mass flow effects were the largest and here again no justifiable explanation could be advanced.

7.6 Schlieren Photographs

The external flow patterns for various duct exit configurations and angles of yaw are given in Figures 9 to 12 inclusive for a Mach number of 1.64 and in Figures 13 to 15 inclusive for a Mach number of 2.04.

At zero angle of yaw completely blocking one duct appeared to have little effect on the intake flow pattern at a Mach number 1.64, Figures 9, a, b, c; however, at a Mach number of 2.04 pronounced boundary layer separation occurred on the forebody on the blocked duct side, Figures 13, a, b, d. This separation sometimes was accompanied by a thickening of the boundary layer on the side of the forebody opposite to the blocked duct, Figures 13b and 13d. Furthermore, separation

appeared to be of an unsteady nature being completely absent in some instances, Figures 13c and d.

At a yaw angle of -2° the unsteady type of separation was observed at a Mach number of 1.64, Figures 10, a, b, c, while at a Mach number of 2.04 separation took place on both sides of the forebody, Figures 14a and 14b.

At larger negative yaw angles separation continued to be unpredictable at both Mach numbers, Figures 11, 12 and 14c. The same phenomenon was observed at positive angles of yaw, Figure 15.

Although vibration of the model, evident in the traces of Figure 3, took place in the pitch plane it could have been responsible for the apparent periodic separation observed optically. This in turn could account for the lack of repeatability in some of the moment measurements mentioned in section 7.5. Presumably the boundary layer on the forebody was laminar and as such was observed to thicken rapidly in some instances. No attempt was made, however, to artifically induce transition in order to delay separation.

7.7 cp Travel

It is apparent from the schlieren observations that the effects of separation on the pressure distribution in the vicinity of the intake entries were appreciable. The resulting effect on cp position was calculated from Figure 16 which gives the variation of C_Y with C_n for alternate blocked duct exit conditions. The actual cp travel is plotted in Figure 17 which shows the position of the cp ahead of the model CG as a percent of the mean aerodynamic chord.

It will be seen that over the yaw angle range considered complete blockage of the starboard duct resulted in a 10% forward movement of the cp, whereas when the port duct was blocked the cp moved backward 4.5%. The fact that these two movements differ in magnitude and sign can probably be attributed to the asymmetry of the model.

8. Conclusions

(a) Blocking the exit of one intake produced a yawing moment tending to rotate the blocked intake into the wind. The change in C_n was about 0.001.

(b) Serious boundary layer separation took place on the forebody on the blocked intake side.

(c) The complete blockage of one intake had an appreciable effect on the mass flow in the other intake, amounting to a reduction of about 8% at zero yaw.

Table 1

Test and Reduced Data for $M_\infty = 2.04$

ψ (Deg)	Config.	Long Sting			Short Sting			Y (lb.)	n_{CG} (lb.in.)	C_Y	C_n
		mV	n_L (lb.in.)	$\frac{p_{ah}}{p_\infty}$	mV	n_s (lb.in.)	$\frac{p_{ah}}{p_\infty}$				
2	0/0	3.4	3.20	0.104	1.9	1.79	0.102	1.14	3.55	0.0080	0.0033
	0/C	2.2	2.07	0.109	0.4	0.38	0.107	1.36	2.49	0.0096	0.0023
	0/½	2.1	1.98	0.105	0.2	0.19	0.110	1.44	2.43	0.0101	0.0023
	C/0	4.5	4.23	0.088	3.9	3.67	0.098	0.45	4.37	0.0032	0.0041
	½/0	5.0	4.71	0.088	3.9	3.67	0.094	0.84	4.97	0.0059	0.0047
	0/0	3.2	3.04	0.092	1.8	1.69	0.096	1.09	3.38	0.0077	0.0032
1	0/0	2.0	1.88	0.104	0.9	0.85	0.102	0.83	2.14	0.0058	0.0020
	0/C	0.8	0.75	0.107	-0.6	-0.56	0.107	1.06	1.08	0.0075	0.0010
	0/½	0.6	0.56	0.104	-0.9	-0.85	0.107	1.14	0.91	0.0080	0.0008
	C/0	3.3	3.11	0.089	2.7	2.54	0.099	0.46	3.25	0.0032	0.0031
	½/0	3.5	3.29	0.088	2.9	2.73	0.095	0.45	3.43	0.0032	0.0032
	0/0	2.1	1.98	0.092	0.8	0.75	0.098	0.99	2.29	0.0070	0.0022
0	0/0	0.7	0.66	0.103	-0.2	-0.19	0.100	0.69	0.87	0.0049	0.0008
	0/C	-0.7	-0.66	0.104	-1.6	-1.51	0.106	0.69	-0.45	0.0049	-0.0004
	0/½	-1.1	-1.04	0.103	-2.0	-1.88	0.107	0.68	-0.83	0.0048	-0.0008
	C/0	1.9	1.79	0.089	1.6	1.51	0.099	0.23	1.86	0.0016	0.0017
	½/0	1.8	1.69	0.088	1.9	1.79	0.095	-0.08	1.67	-0.0006	0.0016
	0/0	-0.2	-0.14	0.091	-0.1	-0.09	0.096	-0.04	-0.15	-0.0003	-0.0001

Table 1 (Continued)

ψ (Deg)	Config.	Long Sting			Short Sting			Y (lb.)	n_{CG} (lb.in.)	C_Y	C_n
		mV	n_L (lb.in.)	$\frac{p_{sh}}{p_\infty}$	mV	n_s (lb.in.)	$\frac{p_{sh}}{p_\infty}$				
-1	0/0	-0.7	-0.66	0.096	-1.1	-1.04	0.099	0.31	-0.56	0.0022	-0.0005
	0/C	-2.0	-1.88	0.104	-2.6	-2.45	0.104	0.46	-1.74	0.0032	-0.0016
	0/½	-2.6	-2.45	0.101	-2.9	-2.73	0.106	0.23	-2.38	0.0016	-0.0022
	C/0	0.3	0.28	0.089	0.7	0.66	0.099	-0.31	0.18	-0.0022	0.0002
	½/0	0.5	0.47	0.088	1.0	0.94	0.094	-0.38	0.35	-0.0027	0.0003
	0/0	-1.3	-1.22	0.092	-1.1	-1.04	0.095	-0.15	-1.27	-0.0011	-0.0012
-2	0/0	-2.1	-1.98	0.100	-2.1	-1.98	0.098	0	-1.98	0	-0.0018
	0/C	-3.5	-3.29	0.101	-3.6	-3.39	0.103	0.08	-3.26	0.0006	-0.0031
	0/½	-4.0	-3.76	0.096	-3.9	-3.67	0.103	-0.07	-3.78	-0.0005	-0.0036
	C/0	-1.2	-1.13	0.089	-0.3	-0.28	0.099	-0.69	-1.34	-0.0048	-0.0013
	½/0	-1.0	-0.94	0.089	-0.1	-0.09	0.095	-0.69	-1.15	-0.0048	-0.0011
	0/0	-2.7	-2.54	0.089	-2.1	-1.98	0.095	-0.45	-2.68	-0.0032	-0.0025
-3	0/0	-3.6	-3.39	0.097	-3.1	-2.92	0.096	-0.38	-3.51	-0.0027	-0.0033
	0/C	-5.1	-4.80	0.100	-4.8	-4.52	0.103	-0.23	-4.87	-0.0016	-0.0046
	0/½	-5.5	-5.18	0.091	-4.9	-4.61	0.103	-0.46	-5.32	-0.0032	-0.0050
	C/0	-2.9	-2.73	0.091	-1.3	-1.22	0.098	-1.22	-3.11	-0.0086	-0.0029
	½/0	-2.2	-2.07	0.091	-1.1	-1.04	0.096	-0.83	-2.33	-0.0058	-0.0022
	0/0	-4.3	-4.05	0.088	-3.0	-2.82	0.093	-0.99	-4.36	-0.0070	-0.0041
-4	0/0	-5.1	-4.80	0.096	-4.0	-3.76	0.096	-0.84	-5.06	-0.0059	-0.0048
	0/C	-6.9	-6.49	0.100	-5.8	-5.46	0.102	-0.83	-6.75	-0.0058	-0.0063
	0/½	-7.0	-6.59	0.093	-5.9	-5.55	0.102	-0.84	-6.85	-0.0059	-0.0064
	C/0	-4.1	-3.86	0.091	-2.2	-2.07	0.098	-1.44	-4.31	-0.0101	-0.0040
	½/0	-3.8	-3.58	0.091	-2.2	-2.07	0.098	-1.22	-3.96	-0.0086	-0.0037
	0/0	-5.5	-5.18	0.089	-4.0	-3.76	0.094	-1.15	-5.54	-0.0081	-0.0052

Table 1 (Concluded)

ψ (Deg)	Config.	Long Sting			Short Sting			Y (lb.)	n_{CG} (lb.in.)	C_Y	C_n
		mV	n_L (lb.in.)	$\frac{p_{sh}}{p_\infty}$	mV	n_s (lb.in.)	$\frac{p_{sh}}{p_\infty}$				
-5	0/0	-6.5	-6.12	0.096	-4.9	-4.61	0.095	-1.22	-6.50	-0.0086	-0.0061
	0/C	-8.5	-8.00	0.099	-7.1	-6.68	0.102	-1.06	-8.33	-0.0075	-0.0078
	0/$\frac{1}{2}$	-8.4	-7.90	0.093	-6.7	-6.30	0.102	-1.29	-8.30	-0.0091	-0.0078
	C/0	-5.4	-5.08	0.091	-3.0	-2.82	0.096	-1.82	-5.64	-0.0128	-0.0053
	$\frac{1}{2}$/0	-5.6	-5.27	0.092	-3.2	-3.01	0.098	-1.82	-5.83	-0.0128	-0.0055
	0/0	-7.5	-7.06	0.088	-5.0	-4.71	0.091	-1.90	-7.65	-0.0134	-0.0072

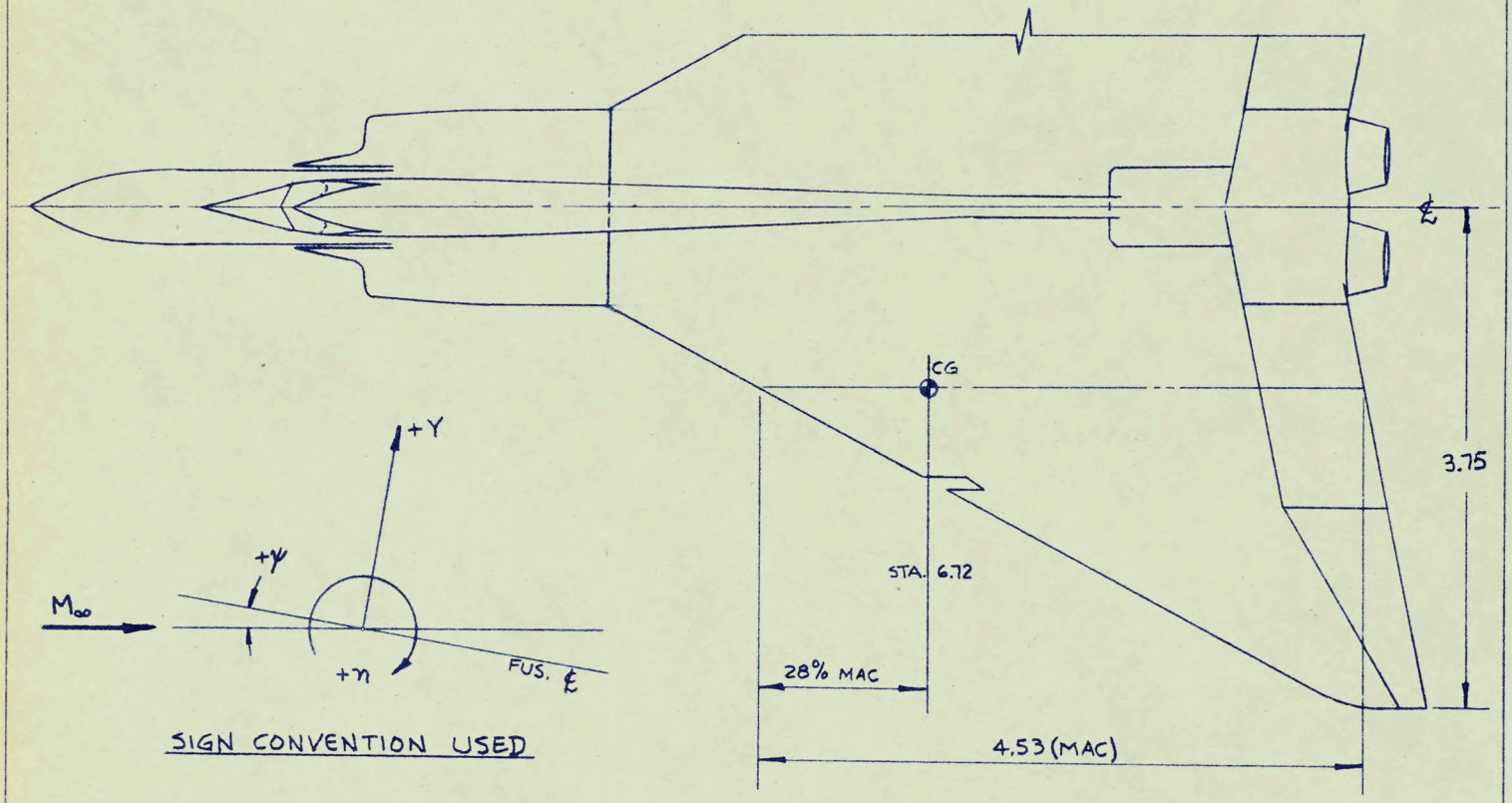

FIG. 1 DIAGRAM OF 1/60 SCALE MODEL

NATIONAL AERONAUTICAL ESTABLISHMENT NO.

LABORATORY MEMORANDUM PAGE OF

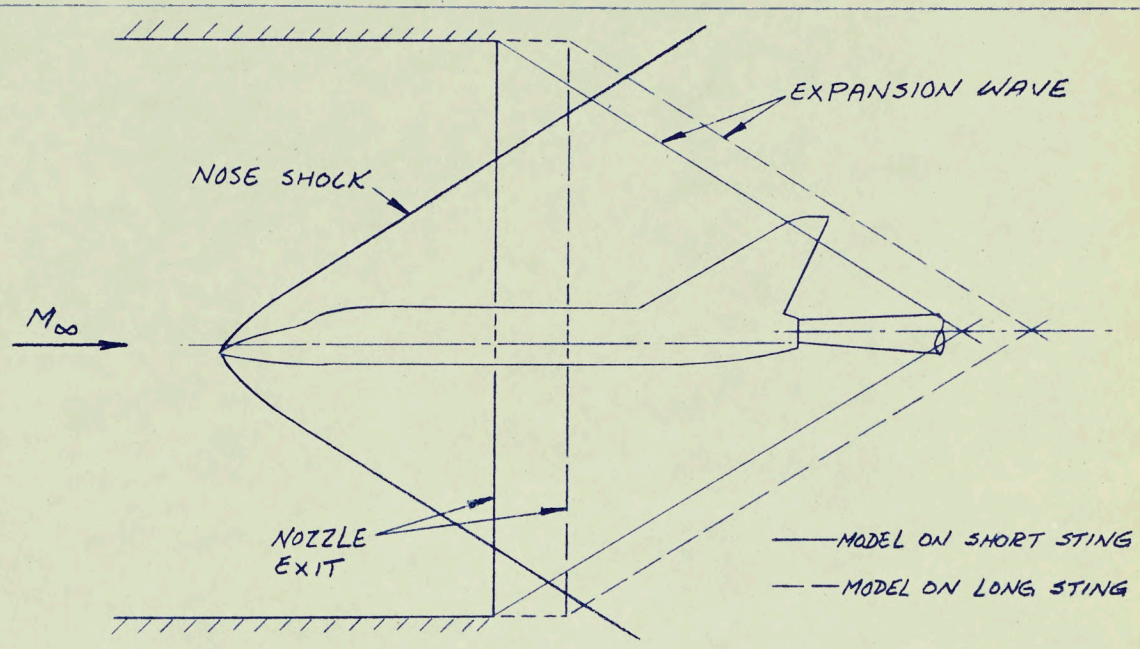

PITCH PLANE

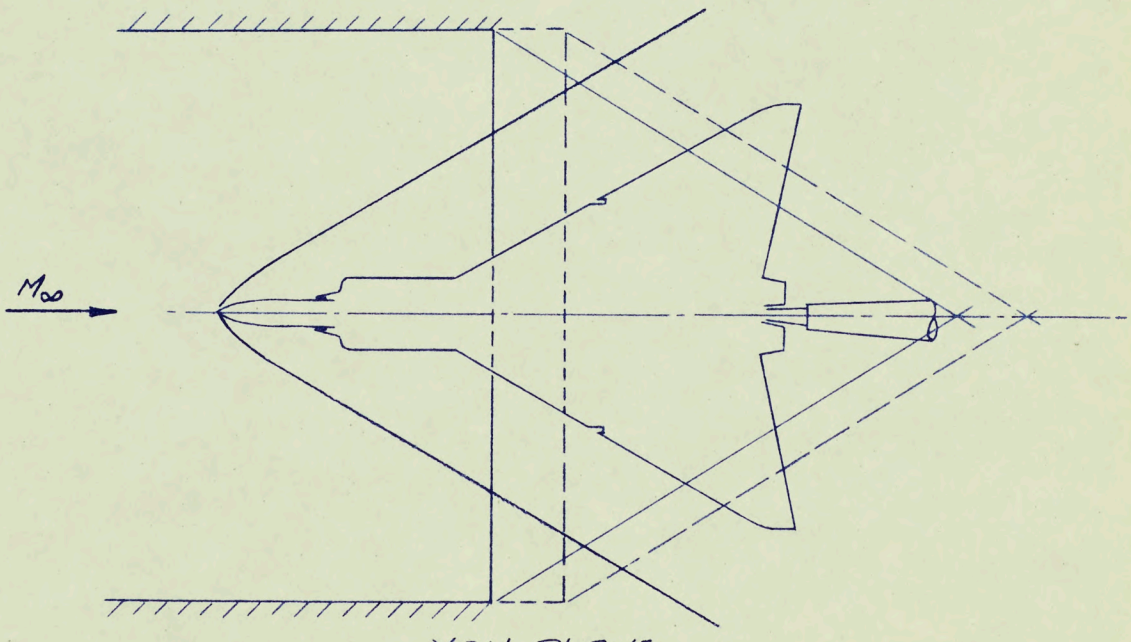

YAW PLANE

FIG. 2 WAVE INTERFERENCE ON MODEL AT $M_\infty = 2.04$

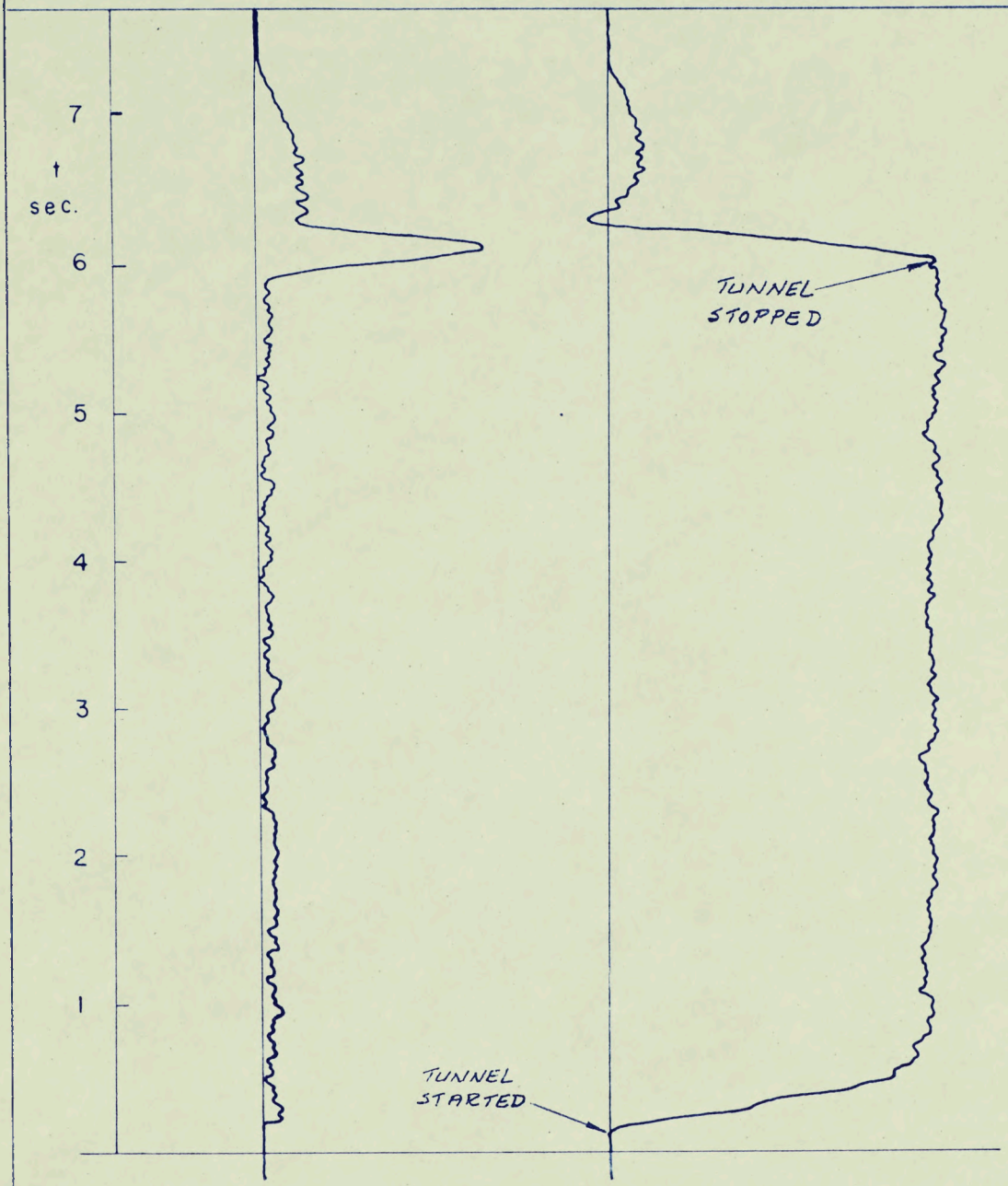

(a) Config. 0/0, ψ =0°, n=-0.19 lb.in.

(b) Config. 0/0, ψ =-5°, n=-4.61 lb.in.

FIG.3 TYPICAL RECORDER TRACES OF MOMENT MEASUREMENTS. M_∞=2.04, MODEL ON SHORT STING.

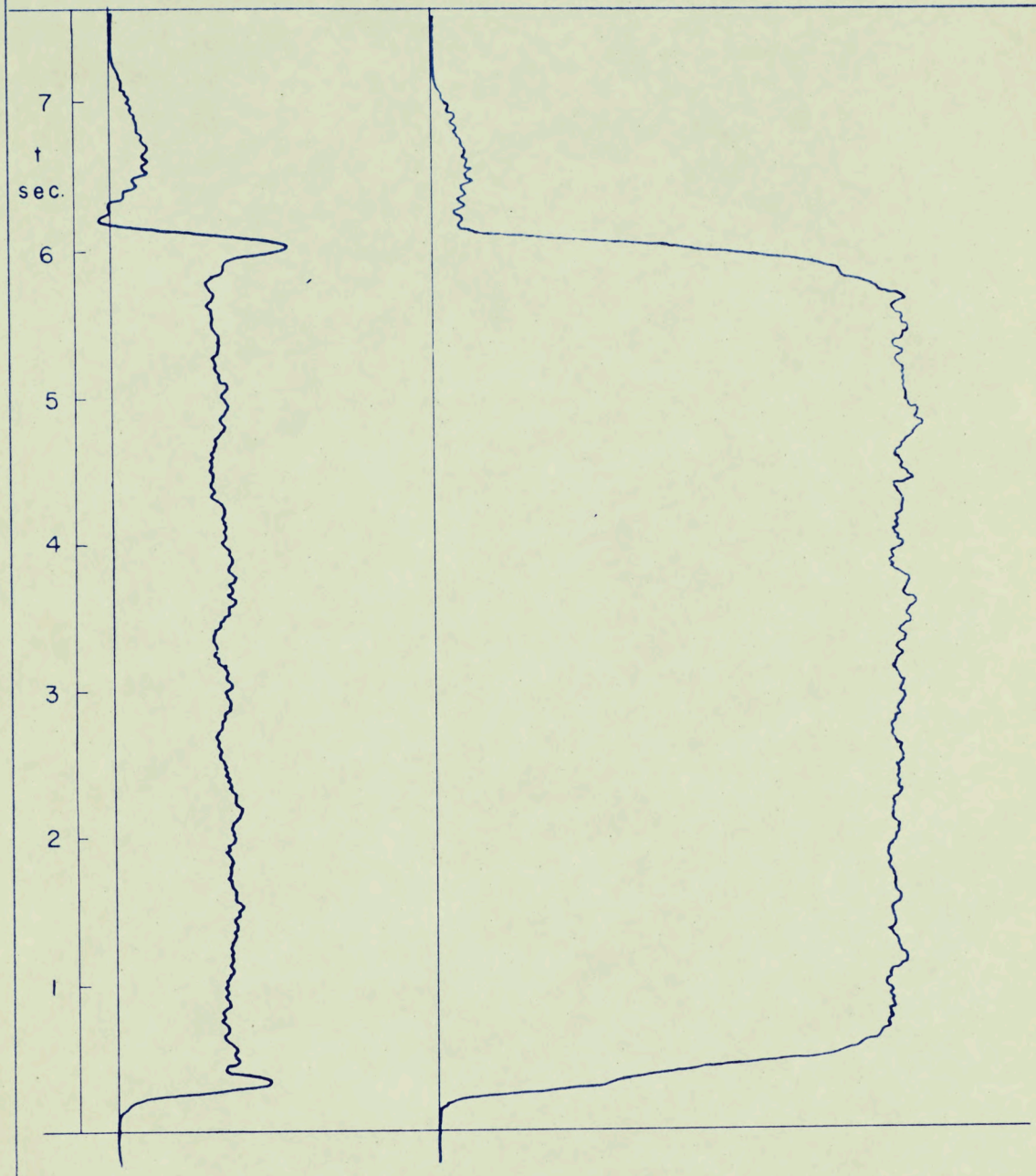

(c) Config. O/C, ψ =0°, n=-1.51 lb.in.

(d) Config. O/C, ψ =-5°, n=-6.68 lb.in.

FIG. 3 (CONCLUDED)

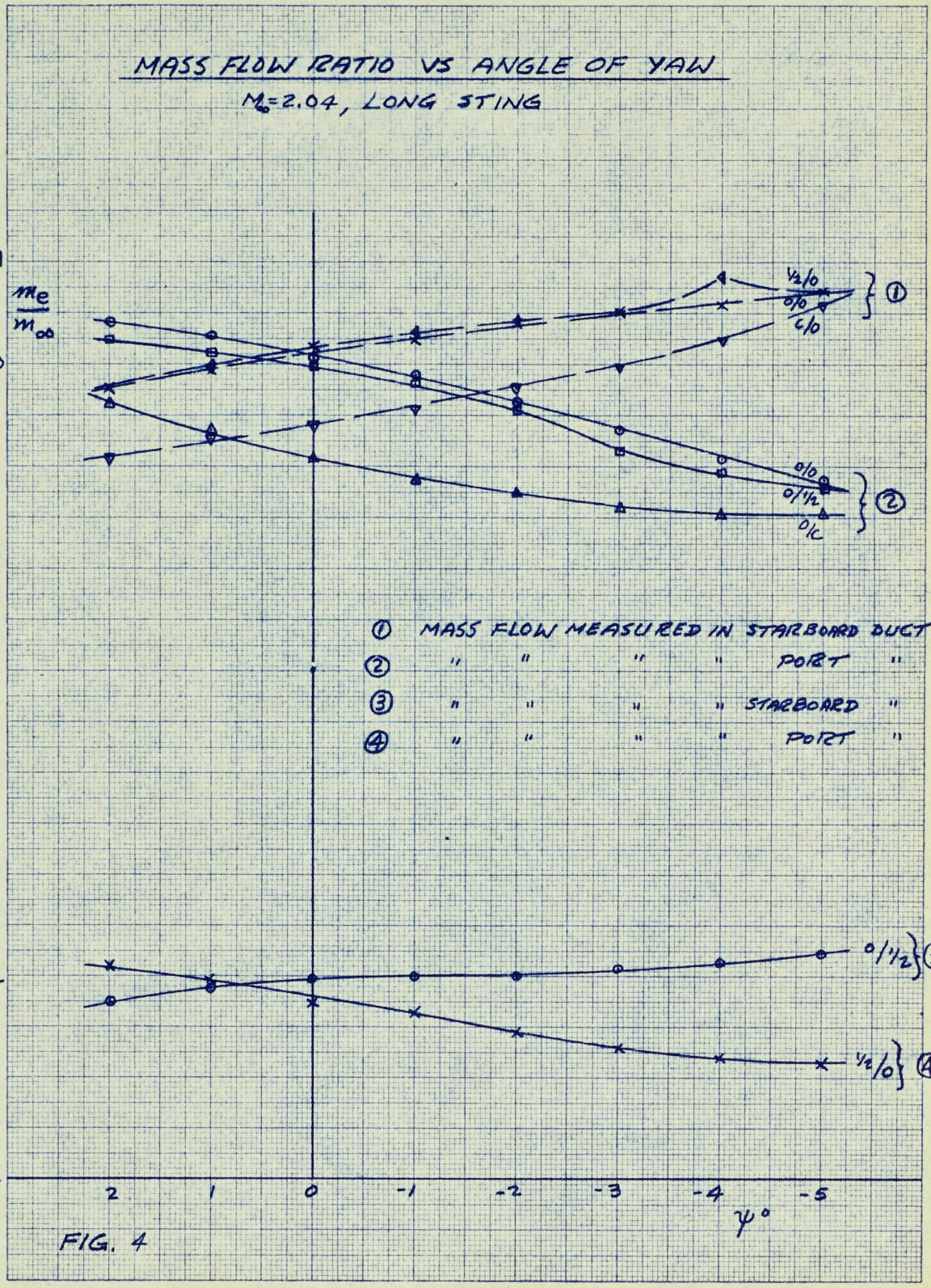

FIG. 4

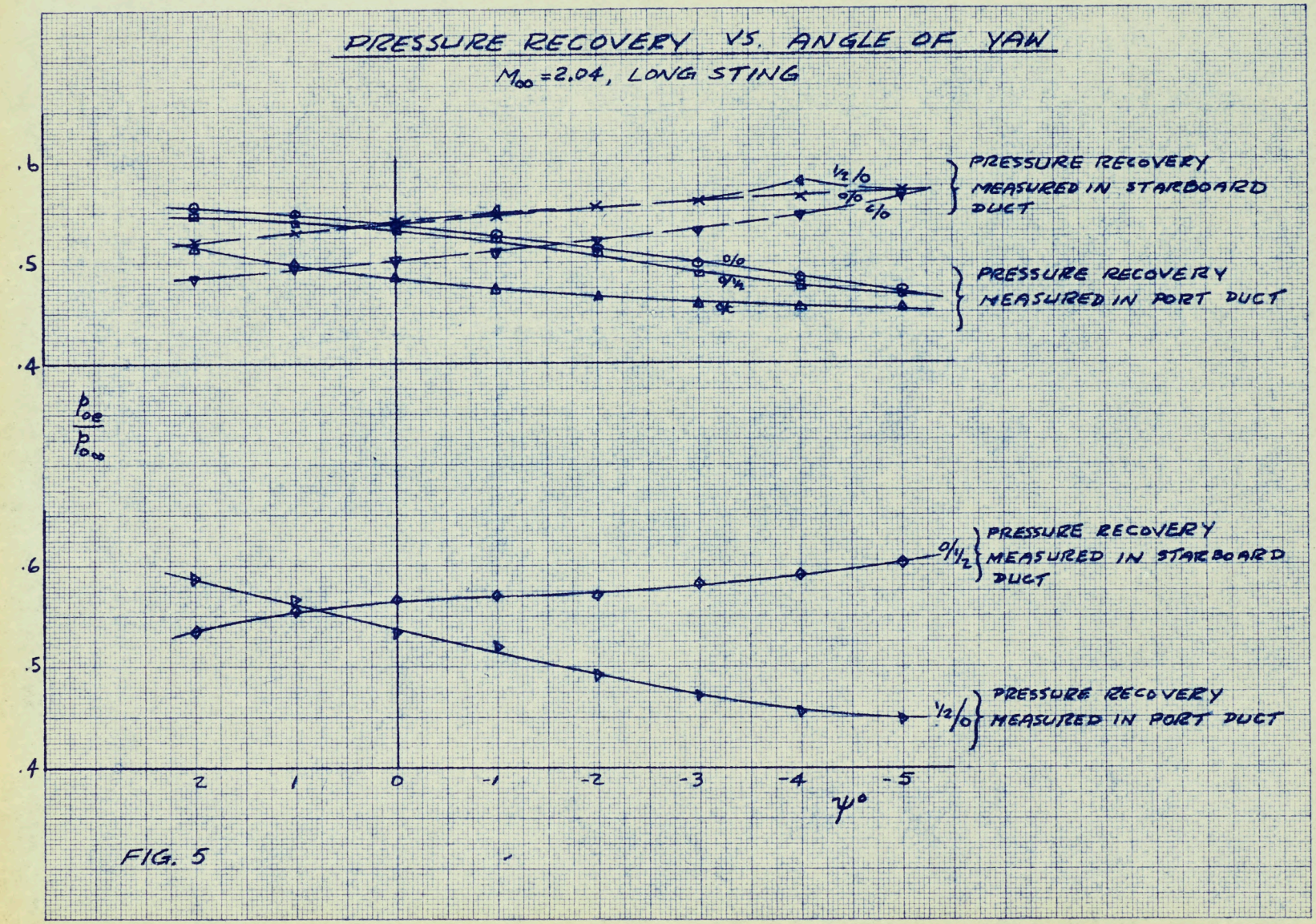

FIG. 5

BASE PRESSURE VS ANGLE OF YAW

$M_\infty = 2.04$, LONG STING ——— SHORT STING — —

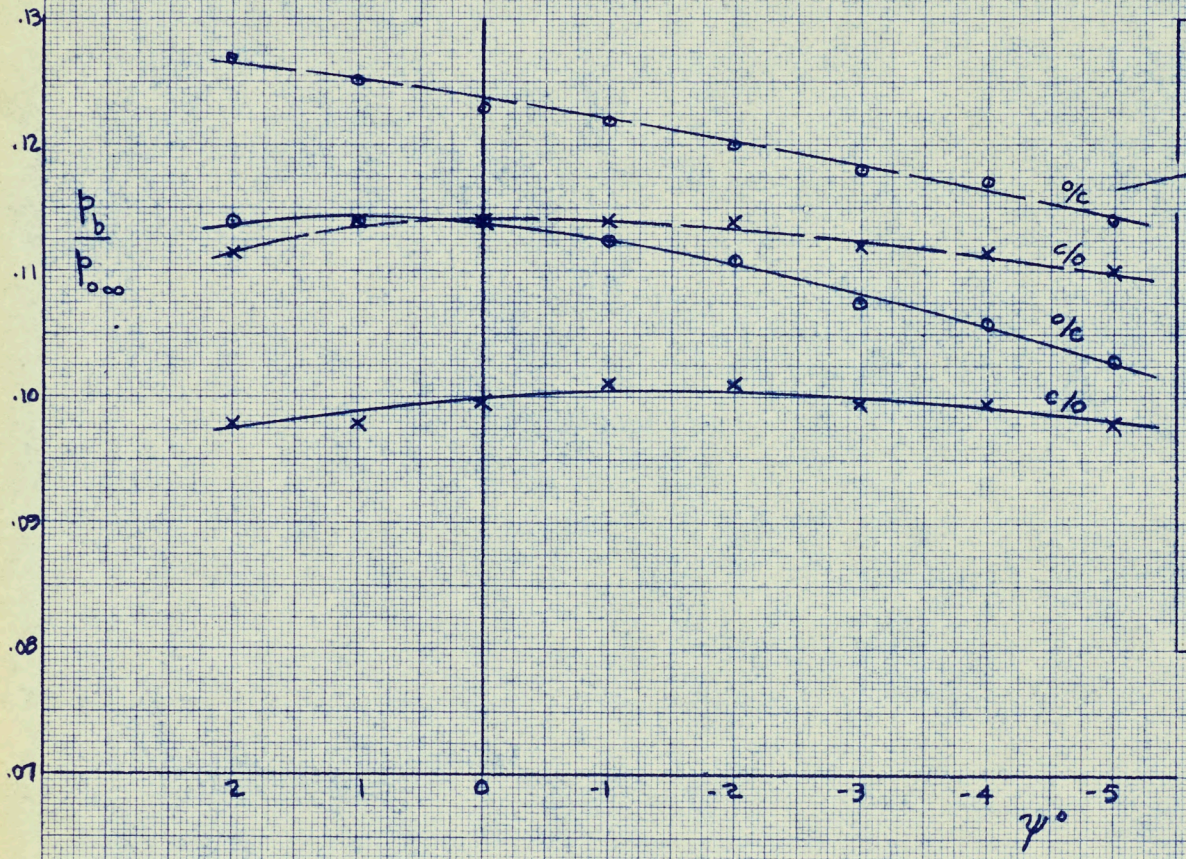

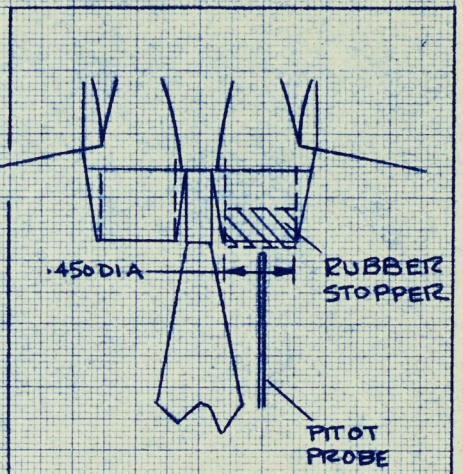

ARRANGEMENT FOR MEASURING p_b WITH CONFIGURATION o/c

FIG. 6

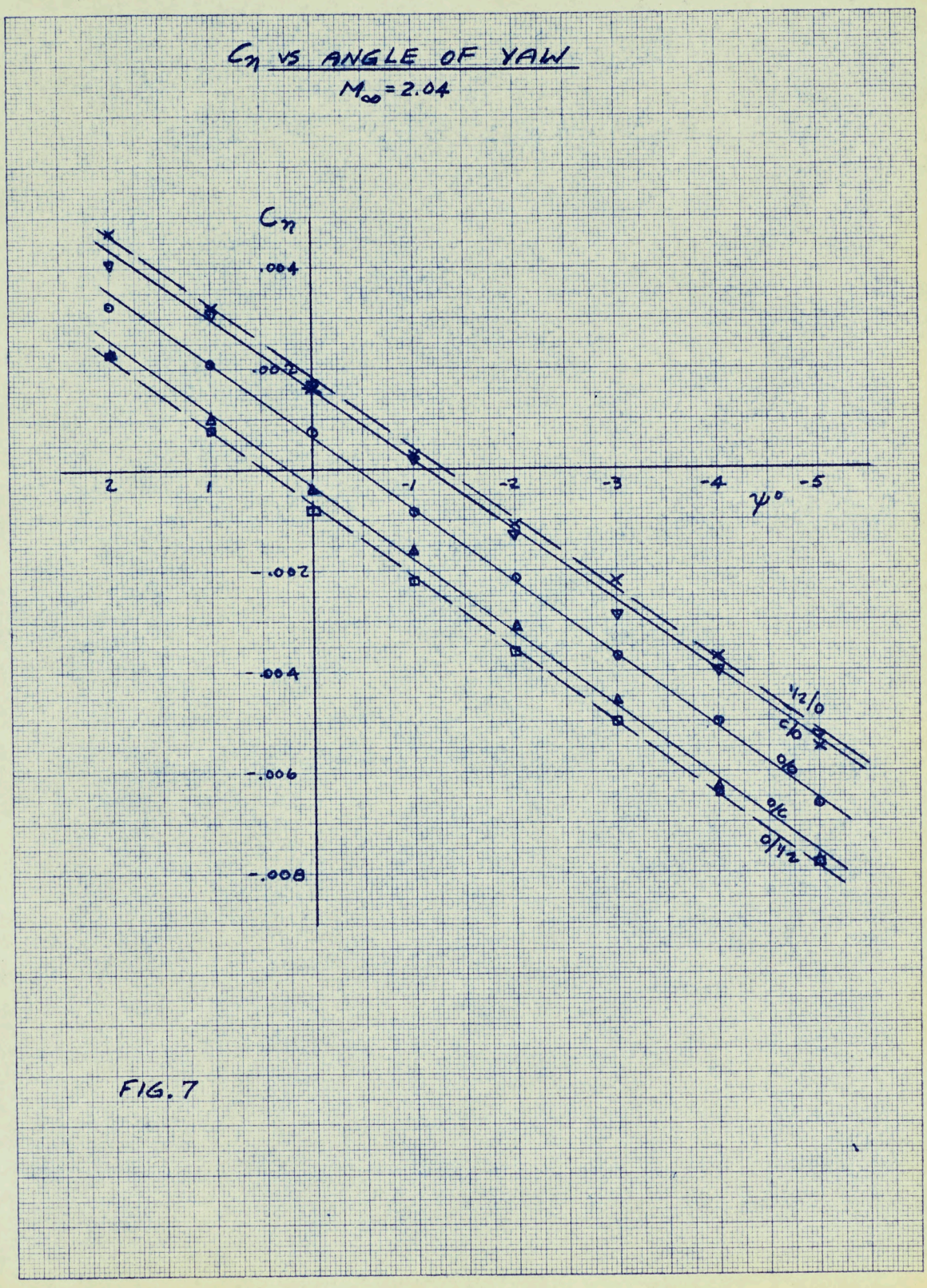

FIG. 7

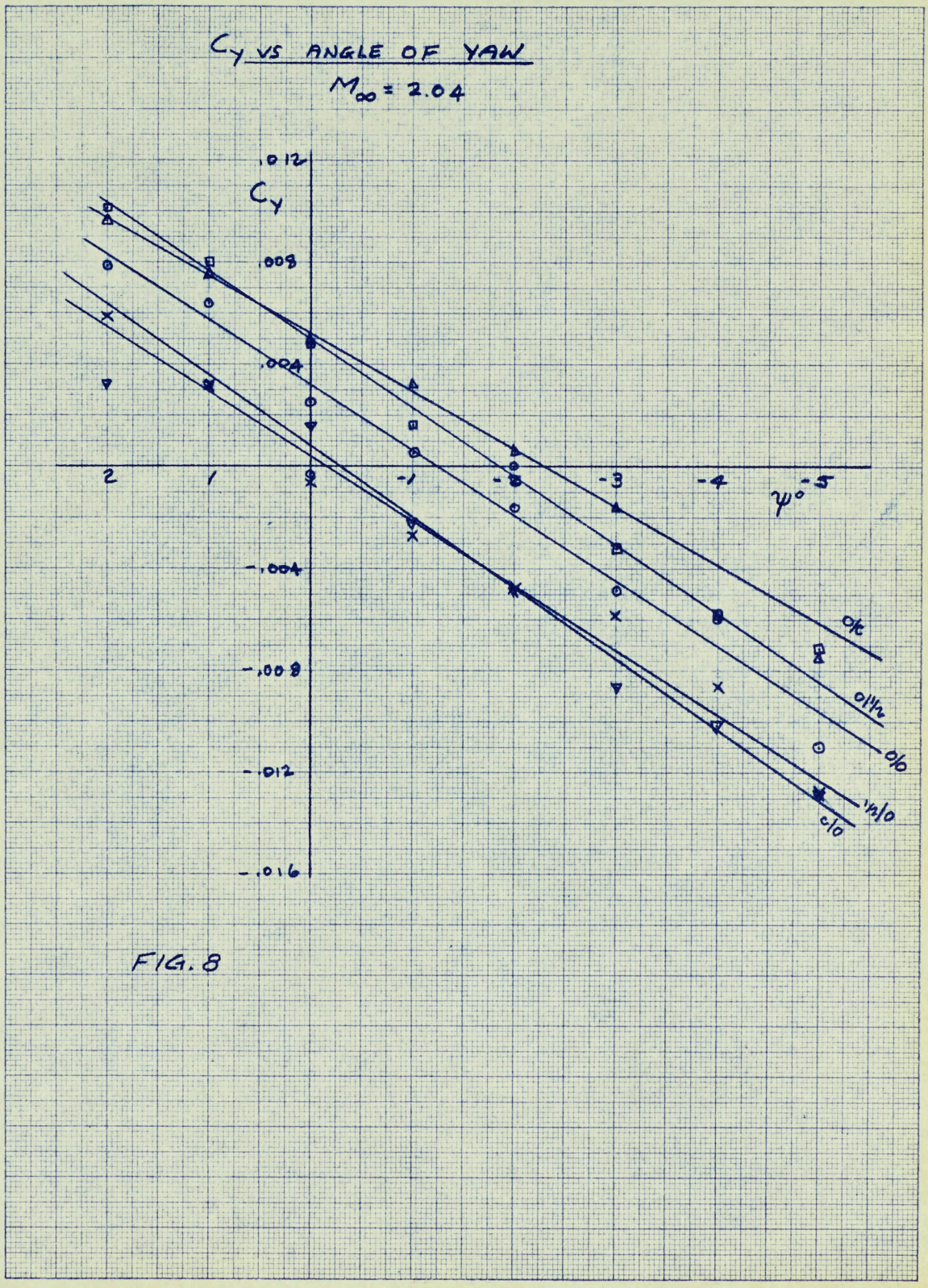

FIG. 8

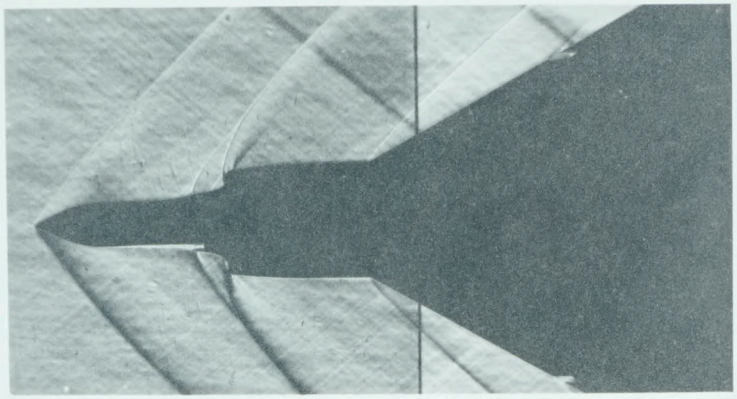

(a) CONFIGURATION O/O

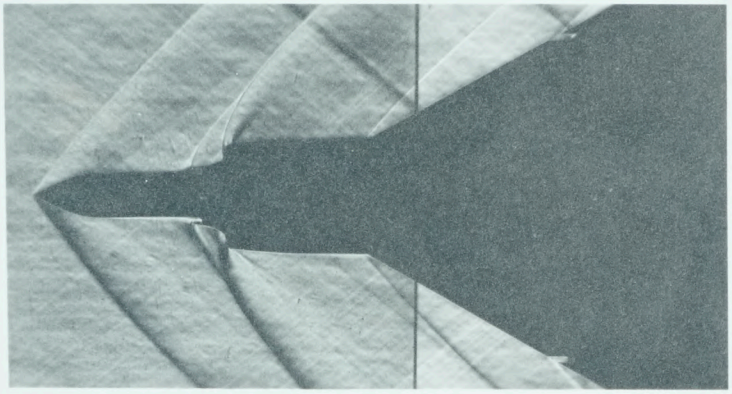

(b) CONFIGURATION O/C

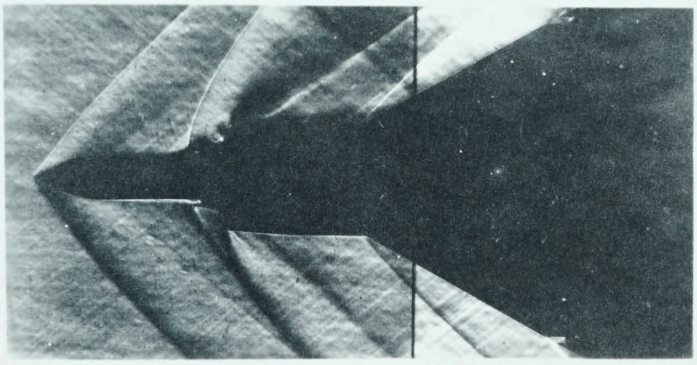

(c) CONFIGURATION C/O

FIG. 9 SCHLIEREN PHOTOGRAPHS $M_\infty = 1.64$, $\psi = 0°$

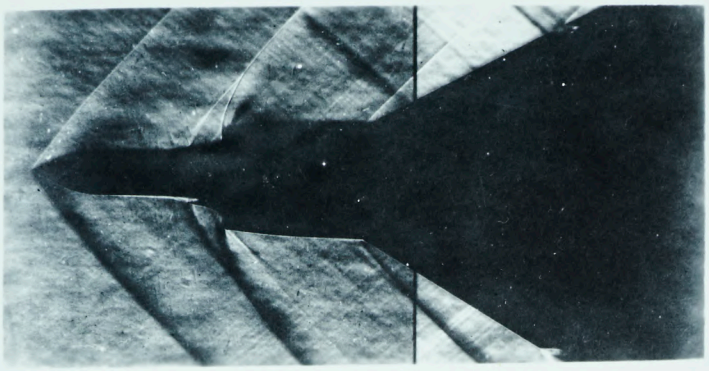

(a) CONFIGURATION O/O

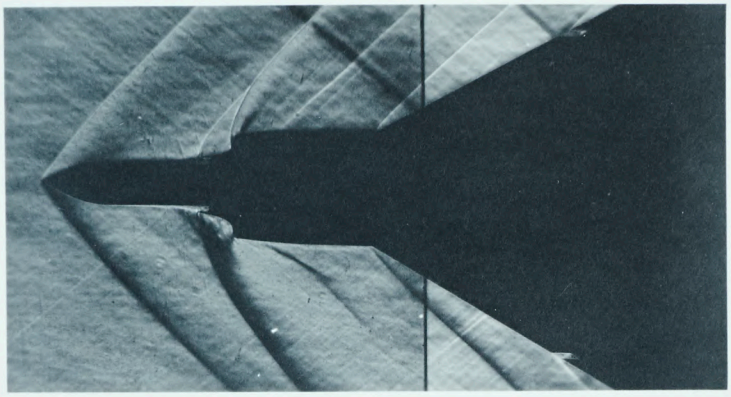

(b) CONFIGURATION O/C

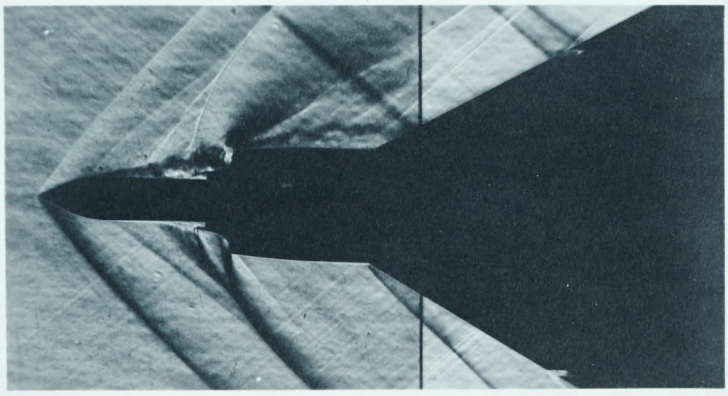

(c) CONFIGURATION C/O

FIG. 10 SCHLIEREN PHOTOGRAPHS $M_\infty = 1.64$, $\psi = -2°$

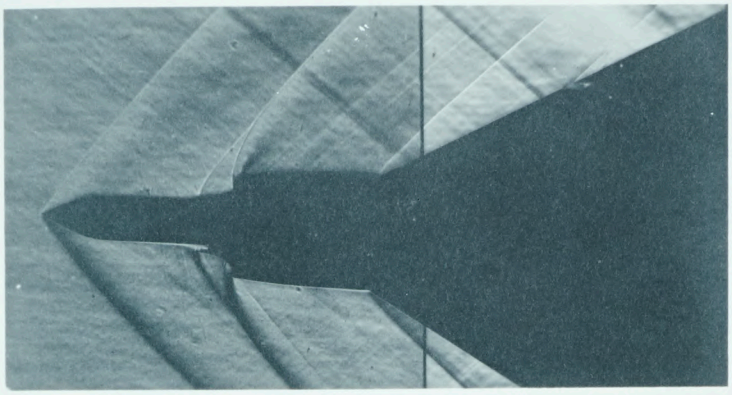

(a) CONFIGURATION O/O

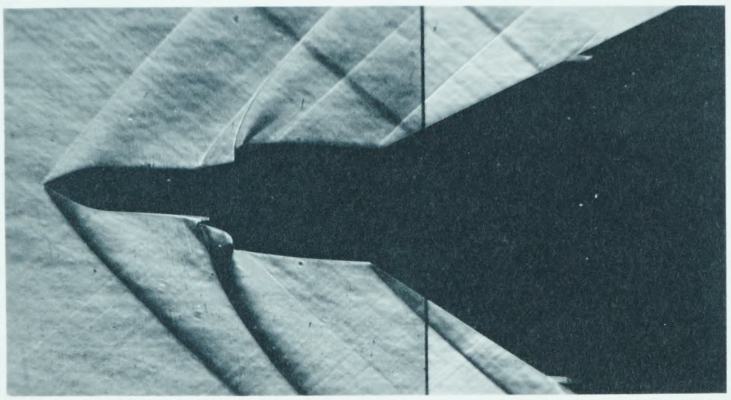

(b) CONFIGURATION O/C

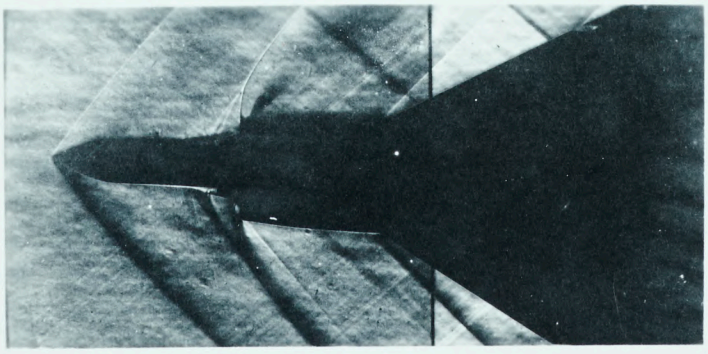

(c) CONFIGURATION C/O

FIG. 11 SCHLIEREN PHOTOGRAPHS $M_\infty = 1.64$, $\psi = -4°$

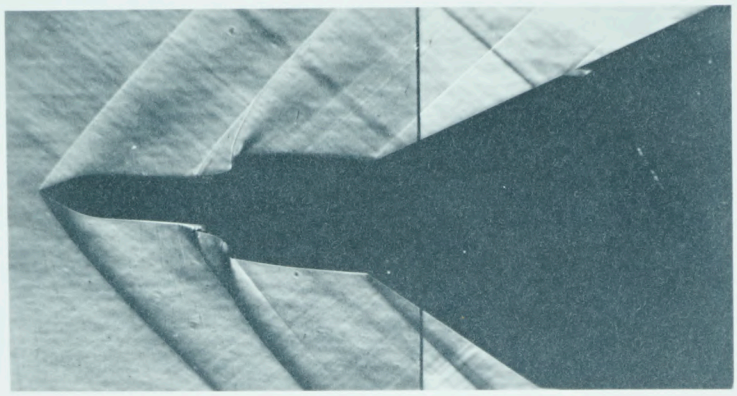

(a) CONFIGURATION O/O

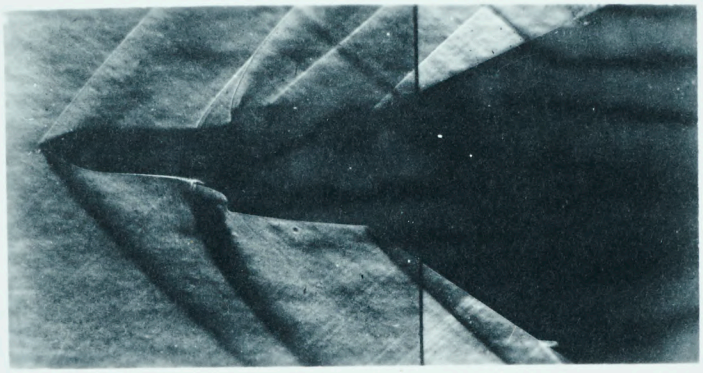

(b) CONFIGURATION O/C

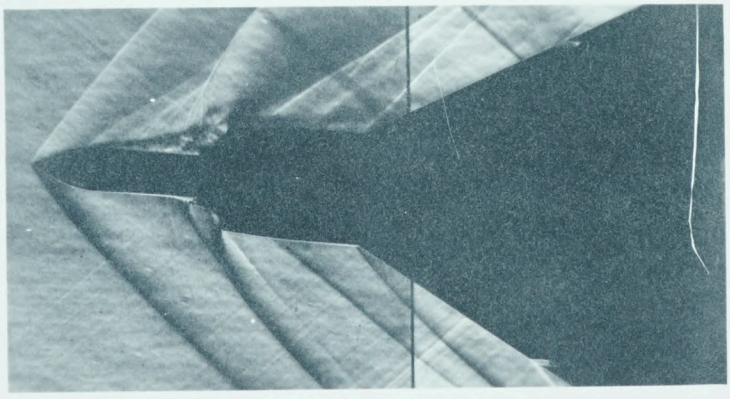

(c) CONFIGURATION C/O

FIG.12 SCHLIEREN PHOTOGRAPHS $M_\infty = 1.64$, $\alpha = -5°$

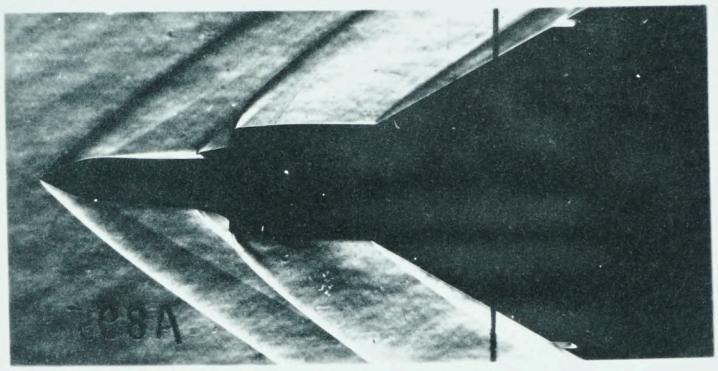

(a) CONFIGURATION 0/0

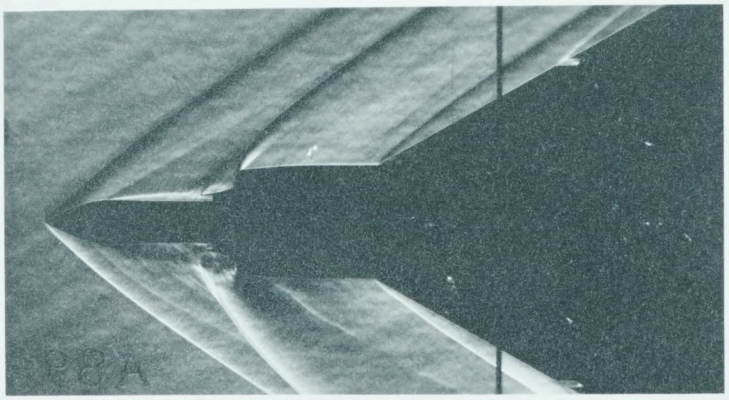

(b) CONFIGURATION 0/C

FIG.13 SCHLIEREN PHOTOGRAPHS $M_\infty = 2.04$, $\psi = 0°$

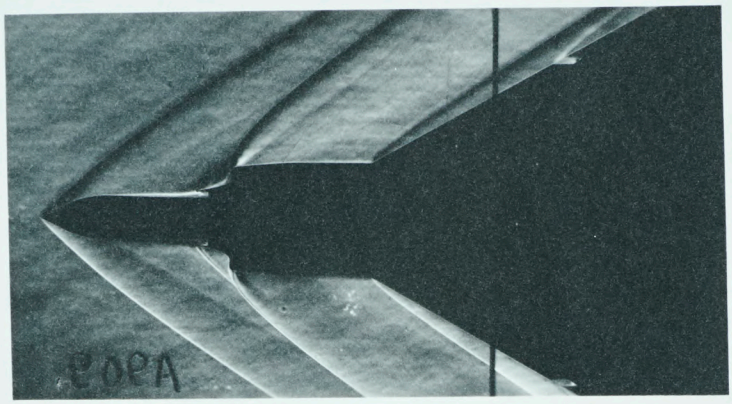

(c) CONFIGURATION C/O

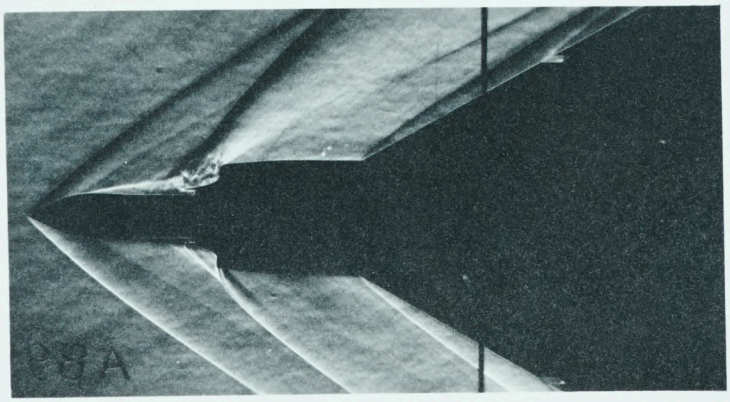

(d) REPEAT OF (c) SHOWING SEPARATION

FIG. 13 (CONCLUDED)

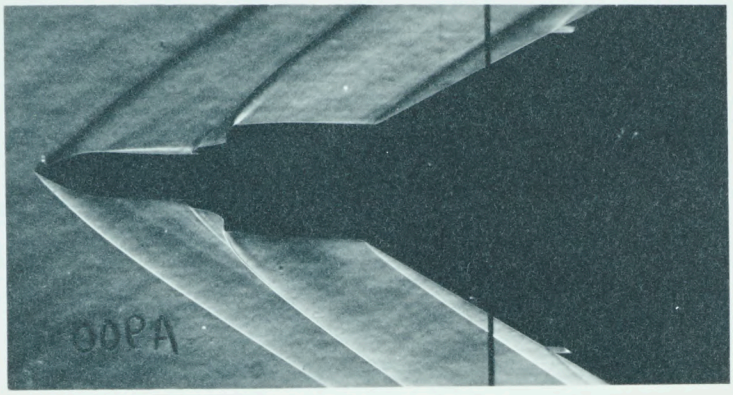

(a) CONFIGURATION 0/0, ψ = -2°

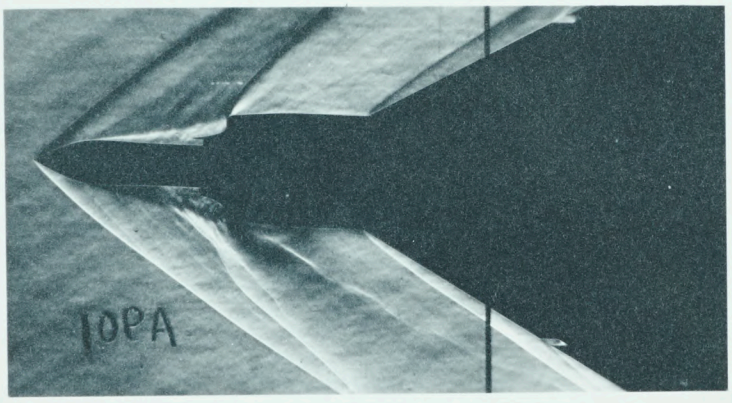

(b) CONFIGURATION 0/0. ψ = -2°

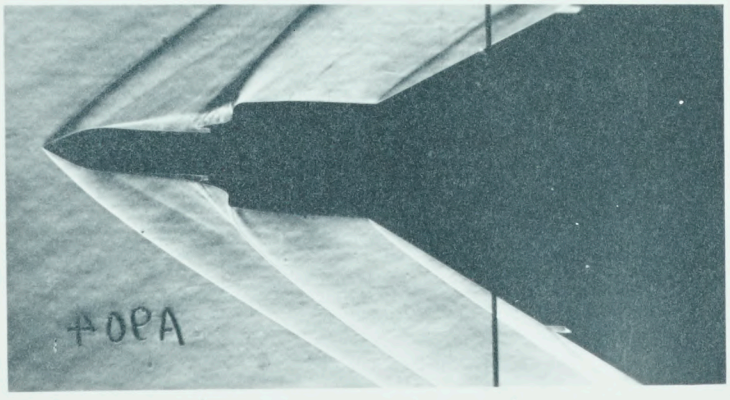

(c) CONFIGURATION C/0, ψ = -3°

FIG.14 SCHLIEREN PHOTOGRAPHS M_∞ = 2.04

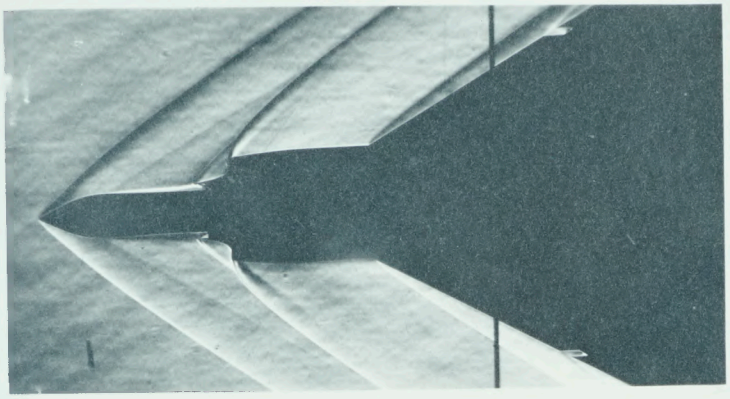

(a) CONFIGURATION O/O

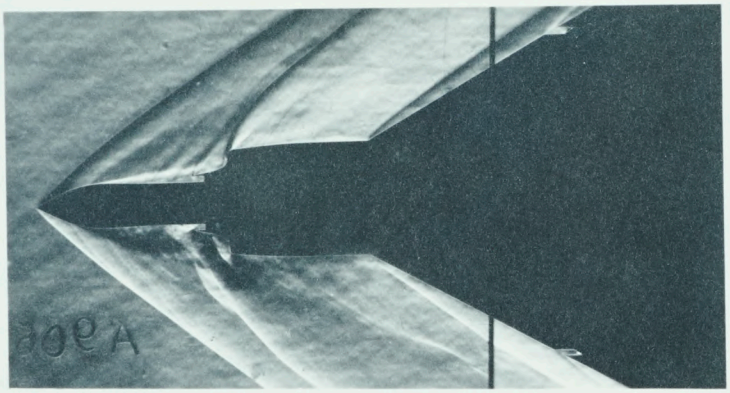

(b) CONFIGURATION O/C

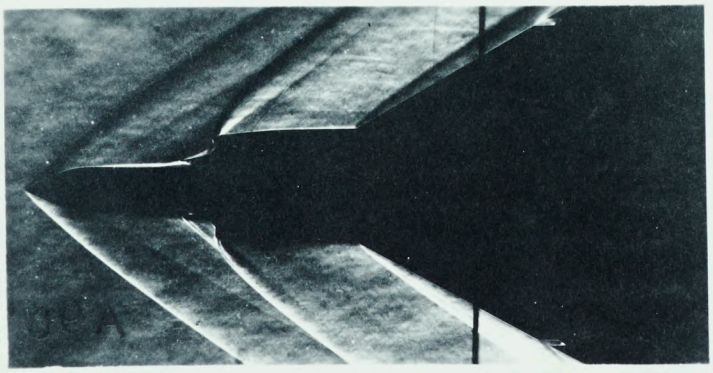

(c) CONFIGURATION C/O

FIG.15 SCHLIEREN PHOTOGRAPHS $M_\infty = 2.04$, $\psi = +2°$

C_y vs C_n

$M_\infty = 2.04$

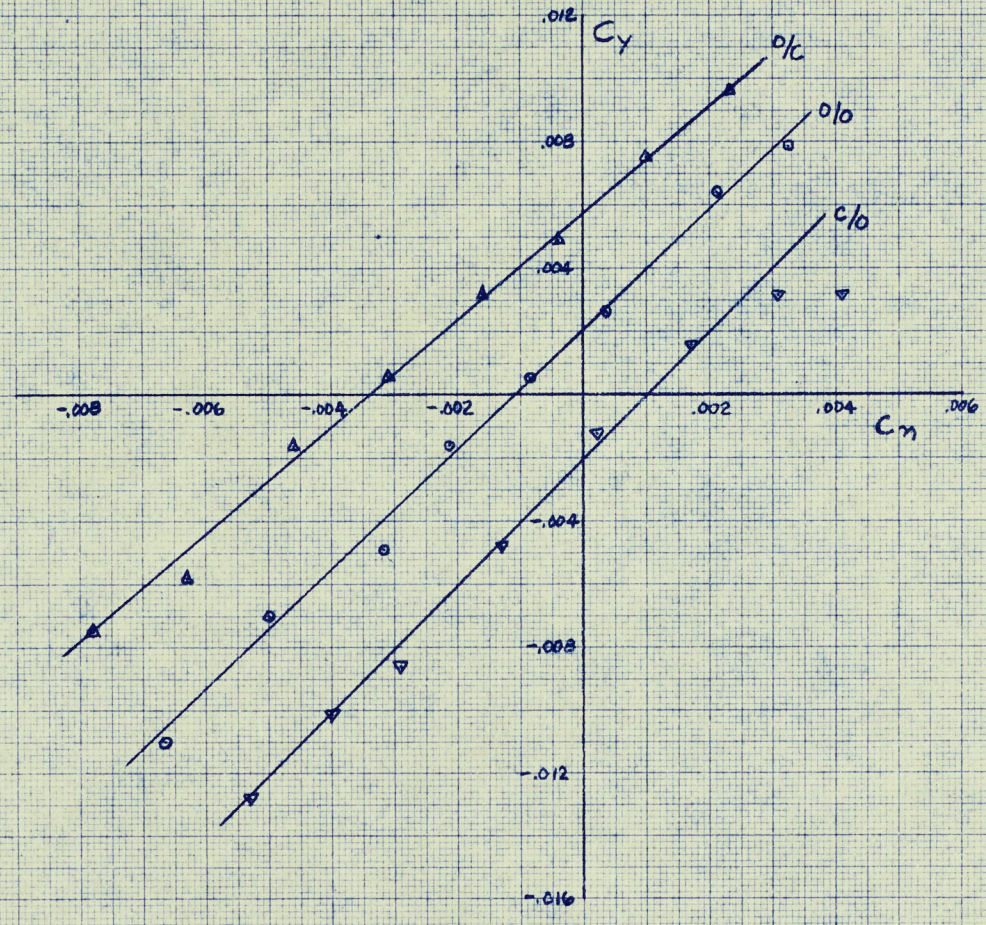

FIG. 16

CP TRAVEL DUE TO INTAKE BLOCKAGE

$M_\infty = 3.04$

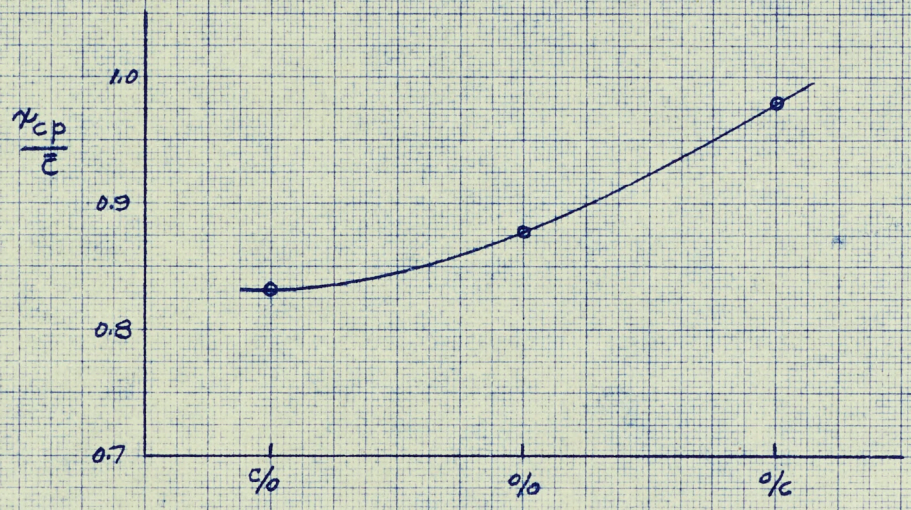

FIG. 17